Optical signatures of bulk and solutions of KC8 and KC24

Damien Tristant, Yu Wang, I.C. Gerber, Marc Monthioux, Alain Pénicaud, Pascal Puech

Optical signatures of bulk and solutions of KC_8 and KC_{24}

Damien Tristant, Yu Wang, Iann Gerber, Marc Monthioux, Alain Pénicaud, and Pascal Puech

Citation: Journal of Applied Physics **118**, 044304 (2015); doi: 10.1063/1.4927291
View online: https://doi.org/10.1063/1.4927291
View Table of Contents: http://aip.scitation.org/toc/jap/118/4
Published by the American Institute of Physics

JOURNAL OF APPLIED PHYSICS **118**, 044304 (2015)

Optical signatures of bulk and solutions of KC_8 and KC_{24}

Damien Tristant,[1,2] Yu Wang,[3] Iann Gerber,[2] Marc Monthioux,[1] Alain Pénicaud,[3] and Pascal Puech[1,a)]

[1]*CEMES-CNRS, UPR-8011, Université Fédérale de Toulouse-Midi-Pyrénées, 29 rue Jeanne Marvig, BP 94347 Toulouse, Cedex 4, France*
[2]*LPCNO, UMR-5215 CNRS, INSA, Université Fédérale de Toulouse-Midi-Pyrénées, Université de Toulouse, 135 Avenue de Rangueil, 31077 Toulouse, France*
[3]*CNRS, CRPP, UPR-8641, Université Bordeaux 1, F-33600 Pessac, France*

(Received 29 May 2015; accepted 12 July 2015; published online 23 July 2015)

We first performed an analysis of the shape of the Raman features of potassium-intercalated graphite at stage 1 (KC_8 GIC) and 2 (KC_{24} GIC), respectively. By varying the excitation energy from ultraviolet to infrared, we observed a sign change of the Fano coupling factor below and above the optical transition related to the shift of the Fermi level which was determined from first principle calculations. This behavior is explained by a sign change in the Raman scattering amplitude of the electronic continuum. The GICs were then dissolved in two different solvents (N-Methyl-2-pyrrolidone and tetrahydrofuran), and the absorbance of the graphenide solutions obtained was measured in the UV range. Two peaks were observed which correspond to the maximum of the computed imaginary part of the optical index. © *2015 AIP Publishing LLC*.
[http://dx.doi.org/10.1063/1.4927291]

I. INTRODUCTION

There is currently a renewal of interest in potassium-intercalated graphite compounds (K-GIC) as they could be used for the scalable production of monolayer graphene. The most heavily potassium-intercalated GIC is the KC_8 compound (designated as stage 1, which corresponds to an assembly of single layers of potassium atoms alternating with single graphenes) whose spontaneous dissolution in suitable solvents[1] allows considering KC_8 solutions as highly interesting for preparing thin films or incorporating graphenes in polymer matrices. The second most heavily K-intercalated GIC is designated as stage 2 and corresponds to an assembly of one layer of potassium atoms intercalated every two graphenes resulting in a stoichiometry of KC_{24}. Considering the color of the resulting K-GIC is a perfect intercalation indicator, as stage 1 appears gold, stage 2 appears blue, and stage 3 appears gray. The optical properties of the bulk compounds have been thoroughly studied through mono-wavelength Raman, reflectivity, or ellipsometry measurements.[2,3] First principle calculations have replaced tight binding models, improving confidence in the electronic band structure results. As potassium is an alkali atom, it shares a large fraction of its last electronic orbital with the neighboring graphenes. Due to this charge transfer, the Fermi level is strongly shifted. This effect drives the optical properties. From angle-resolved photoemission study of KC_8,[4] a shift of the Fermi level of 1.35 eV has been determined in full agreement with first principle calculations. As a consequence, the optical transition is equal to 2.7 eV, i.e., twice the Fermi level shift. Raman spectroscopy is a powerful tool for investigating many aspects related to structural, textural, and properties of carbon materials. For instance, for single wall carbon nanotubes, it is able to determine the tube diameter,[5] the semiconducting or the metallic nature through van Hove resonance,[6] and the doping level;[7] for graphene, it is widely used to determine the doping level,[8] the number of layers,[9] or the type and amount of defects.[10,11] In geology, the Raman signature of carboneous material can be used as a geothermometer.[12] The Raman signal allowed in the center of the Brillouin zone corresponding to the phase opposition motion of bonded atoms is degenerated. It is called G or E_{2g} mode. This mode interacts with electrons or charges provided by a current flow or doping for example. In graphite intercalated compound, the graphite G band is replaced by a coupled mode between electrons and phonons. The non-adiabatic effects shift the optical mode by 311 cm^{-1} to be compared to the G band wavenumber for genuine graphite (1581 cm^{-1}). Moreover, the shape of the mode is modified by a coupling with the incoming photons, inducing a Fano shape. This is where more knowledge is needed. The optical mode in GIC has been studied versus various parameters such as high pressure[13] or during intercalation.[14] Indeed, the variation of the Fano shape in graphene with respect to a large range of excitation energy has not been studied in detail so far. Also, when the GICs are dissolved, the Raman signature of the material becomes weak and complementary techniques should be used. In this paper, we report both a Raman study using UV to infrared excitation wavelengths and an optical transmission study of KC_8 and KC_{24} GICs in solution. The coupling factor of the Fano profile is analyzed. In order to fully discuss our experimental observations and also the literature data, optical indexes were determined by means of first principle calculations allowing the absorption peaks visible in the UV range to be explained.

II. EXPERIMENTAL CONDITIONS

The samples were prepared using a modified vapor-phase reaction procedure that produces alkali metal-intercalated

a)Electronic mail: Pascal.Puech@cemes.fr

graphite flakes with well-controlled intercalation stages.[2,3,15] Graphite and potassium were separately placed in opposite ends of a Pyrex tube under inert atmosphere, and the tube was evacuated down to 10^{-4} mbar and then sealed. The tube was placed for 3 days in a two-zone furnace where graphite and potassium were maintained at different temperatures, T_G and T_1, respectively. T_G is maintained at 250 °C in order to have a high enough potassium vapor pressure and a satisfactory reaction rate for the intercalation reaction. By adjusting the temperature difference $T_G - T_1$, stage 1 and stage 2 potassium intercalated compounds were, respectively, obtained. They were qualitatively identified by their golden and blue color, respectively.[3] For Raman analysis, the samples were placed in sealed cuvettes and the color of the GIC flakes under study was visually verified before the measurements. An objective with long working distance was used. The laser power was always kept below the value known for promoting desintercalation, typically selecting a value of 2 mW with a magnification objective of ×40. Raman spectra were acquired with various spectrometers (UV Dilor, T64000 Jobin-Yvon Horiba, visible Dilor, XPlora Jobin-Yvon Horiba) depending on the available laser sources. The solution has been prepared according to literature.[1] Intercaled compounds are dissolved at room temperature in N-Methyl Pyrrolidone (NMP) or TetraHydroFuran (THF) under inert atmosphere and stirring. Then, mild centrifugation is used to remove insoluble material. Absorption spectroscopy was performed on these solutions with a Unicam UV4-100 spectrometer from 200 to 900 nm.

III. COMPUTATIONAL DETAILS

We have performed total-energy Density Functional Theory (DFT) calculations with the Vienna *ab initio* simulation package VASP,[16–19] within the full-potential projector augmented wave (PAW) framework.[20,21] The plane-wave basis set cutoff energy was set to 400 eV, with a Gaussian smearing of 0.005 eV width, in order to assure well-converged total energy and force values. All atoms have been fully relaxed until the forces on individual atoms were smaller than 0.01 eV/Å^{-1}. The calculation cell used for stage 1 (KC_8) contained one layer of 8 C atoms and 1 K atom [electronic VASP configuration (Ne) $3s^2 3p^6 4s^0 3d^1$] and two layers (AB-stacking is energetically the most favorable) of 24 carbon atoms and 2 potassium atoms for stage 2 (KC_{24}). The cell shape and volume were also allowed to relax; in fact, the c-axis separation of intercalate potassium layers, 5.19 Å (stage 1) and 7.87 Å (stage 2), respectively, are in a good agreement with the experimental values.[22] The nonlocal correlation effects were treated by the vdW-DF functional[23] in the recent vdW-DF2 form.[24] In conjunction with the present correlation functional, we have followed the requirement of Klimes *et al.*[25] regarding exchange functional without spin-polarization. The k-point sampling was always based on a Γ-centered grid for all types of calculations. A $(13 \times 13 \times 7)$ grid for stage 1 and $(11 \times 11 \times 5)$ for stage 2 was used to optimize the structure. $(13 \times 13 \times 9)$ and $(11 \times 11 \times 7)$ grids were used to determine the charge transfer and band structure for stages 1 and 2, respectively. Bader charge analysis[26] was used to estimate charge transfer using the Henkelmans group program.[27–29] Our calculated macroscopic dielectric constants using the Kohn-Sham independent-particle picture were collected by using a $(11 \times 11 \times 5)$ grid for stage 1 and $(7 \times 7 \times 5)$ for stage 2.

IV. FANO PROFILE

If a Raman active transition is allowed for both a pure phonon (ω_0) and a continuum with a density of levels $\rho(E)$ coupled through an interaction of strength V, a Fano shape may be observed. In the following, $\pi^{-1}\ R(E)$ is the Hilbert transform of $\rho(E)$. The Fano profile[30] used to fit the data associated to stages 1 and 2 could be expressed as[30]

$$I = I_0 \frac{\left(1 + \frac{\omega - \Omega}{q\Gamma}\right)^2}{1 + \left(\frac{\omega - \Omega}{\Gamma}\right)^2}, \tag{1}$$

where Ω is the renormalized wavenumber of the coupled state ($\Omega = \omega_0 + V^2 R(E)$), Γ is linked to the lifetime of the coupled state ($\Gamma = \pi V^2 \rho(E) + \gamma$) with γ corresponding to the intrinsic broadening, $I_0 = \pi\rho(E)T_e^2$ and q is the coupling parameter given by[31]

$$q = \left(V\frac{T_p}{T_e} + V^2 R(E)\right) \times \frac{1}{\pi V^2 \rho(E)}, \tag{2}$$

where T_e and T_p are the Raman scattering amplitudes of the electronic continuum and the decoupled phonon, respectively. The lifetime Γ depends on the free-carrier concentration but not on the excitation energy. This is a constant value. The coupling factor q is a function of both the laser wavelength through the $\frac{T_p}{T_e}$ ratio and the free-carrier concentration through $R(E)$.[32] Usually, the coupling factor keeps the same sign and changes are not easily accessible with semiconductor like diamond[33] or silicon.[34] In our case, the phonon in KC_8 and KC_{24} is, strictly speaking, already a coupled mode due to non adiabaticity.[35]

V. RESULTS AND DISCUSSION

Raman scattering experiments were carried-out on bulk stage 1 and stage 2 K-GICs. In Figure 1 are reported the Raman spectra of KC_8 with the excitation energy ranging from 3.71 to 2.61 eV. The shape of the Raman spectra was well fitted by Fano line profiles, which are also reported (red lines) in the figure.

For KC_{24}, Figure 2 shows the Raman spectra for the excitation energy ranging from 2.41 to 1.58 eV. For the spectrum at 1.58 eV, the reported fit was made considering only one Fano line and the wavenumber range beyond 1530 cm^{-1}. By this way, the inflexion is well reproduced. However, several Fano lines should be considered for obtaining a good fitting as already mentioned in the literature,[36] and adding other components actually lead to a perfect fitting (not shown).

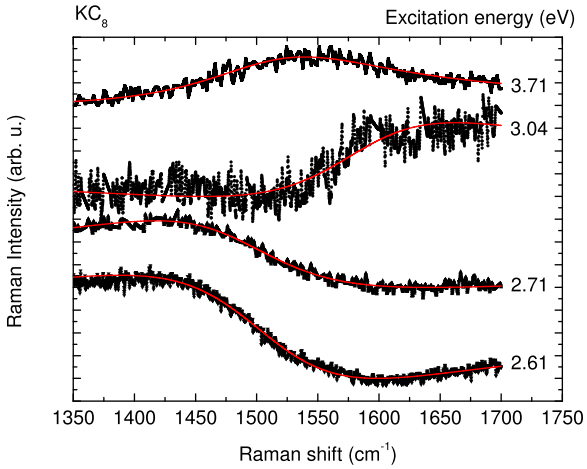

FIG. 1. Raman spectra around the optical transition for KC_8. The fitting (Fano) lines are in red.

From the fittings, we have extracted the q coupling factor parameter. This parameter is interesting as we can see an inversion in the background in both Figures 1 and 2. For high excitation energies, the background is more intense above the phonon energy. On the contrary, for low excitation energies, the background is more intense below the phonon energy. This inversion in the background intensity is due to the sign inversion of the coupling factor q. Consequently, we have plotted the q factor versus the excitation energy for KC_8 and KC_{24} in Figures 3 and 4, respectively.

Ignoring the lifetime, the expression of T_e and T_p close to the transition energy ($\omega_L = \omega_f - \omega_i$) could be expressed by[37–39]

$$T_e \propto \frac{1}{(\omega_f - \omega_i) - \omega_L} \tag{3}$$

and

$$T_p \propto \frac{1}{[(\omega_f - \omega_i) - \omega_L]^2}, \tag{4}$$

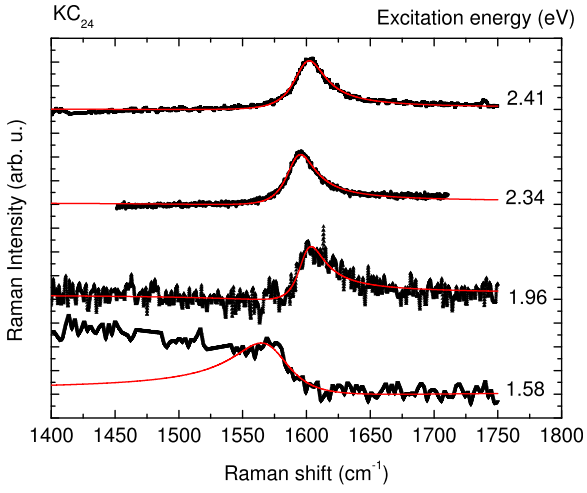

FIG. 2. Raman spectra around the optical transition for KC_{24}. The fitting (Fano) lines are in red.

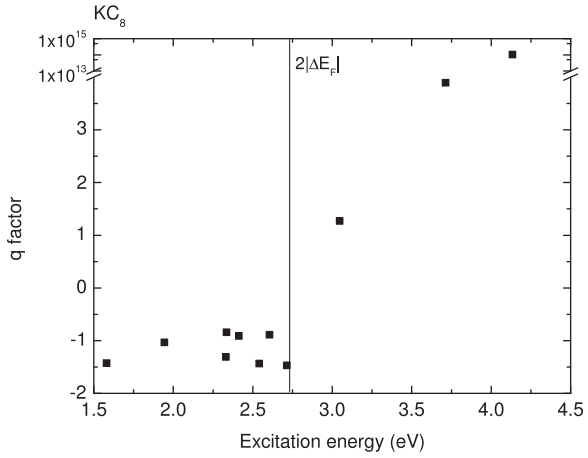

FIG. 3. Coupling factor q versus the excitation energy for KC_8. The vertical line indicates the position of the optical transition ($2\,|\Delta E_F|$) associated to the transition between occupied valence band state to first unoccupied conduction band state.

where ω_L is the wavenumber of the scattering light and $\omega_f - \omega_i$ is the wavenumber of the electronic transition (i for initial to f for final).

The full calculation considering all pathways has been already done for T_p.[40,41] By ignoring the lifetime, the sign of the phase of T_p is constant.[40] Consequently, the sudden sign change of q is due to T_e. In the denominator of the Raman scattering amplitude of the electronic continuum in Eq. (3), when crossing the transition energy, the sign switches. Far from the transition, as the electronic band structure is quite complex at an energy higher than the transition energy (see the band structure reported in Figure 5), the full calculation of $\frac{T_p}{T_e}$ ratio and thus of q is difficult. Indeed, the exact expression of the coupling factor q is not straightforward. For example, with silicon, a sign change of q was expected at 3.4 eV (E_1 transition).[37] However, in this case, because the background change was small and actually observed from 3.8 eV only,[34] and since the intensity above 3.7 eV is also related to the E_2 transitions,[42] there was some doubt left regarding the actual sign change of q. In our case, however, we observed clearly this sign change around the optical

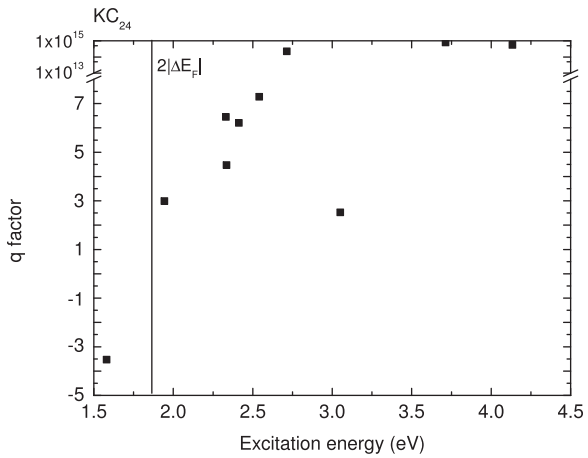

FIG. 4. Coupling factor q versus the excitation energy for KC_{24}. The vertical line indicates the position of the optical transition ($2\,|\Delta E_F|$) associated to the transition between occupied valence band state to first unoccupied conduction band state.

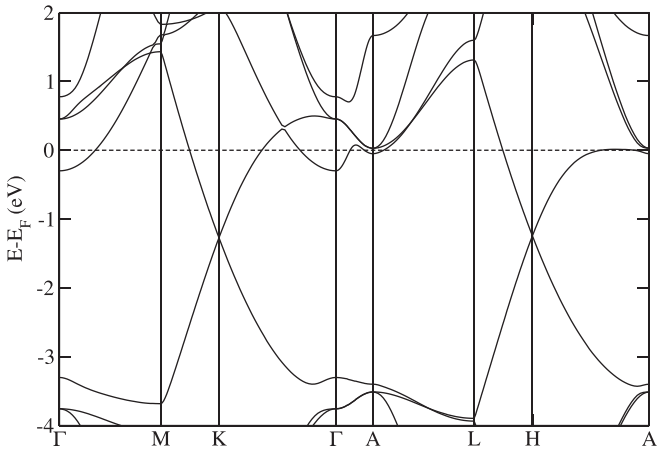

FIG. 5. Calculated electronic band structure of KC_8.

transition for KC_8. This compound has a quite simple band structure with a Dirac cone around the K point.

From *ab-initio* calculations and Angle-Resolved PhotoEmission Spectroscopy (ARPES) experiments,[4] the Fermi level shift is 1.35 eV, giving a transition energy at 2.7 eV. Our calculations reported in Figure 5 give the same value. The coupling factor q changes between 2.71 and 3.04 eV. Below 2.71 eV, the q value is negative. Adding the phonon contribution ($\hbar\omega_G/2$), the Raman transition energy reaches 2.8 eV, which does not change much the discussion. As the $\frac{T_p}{T_e}$ ratio changes around $2|\Delta E_F|$, this term dominates in the coupling factor q. The wavenumber shift of the renormalized phonon could be used to determine the value of $V^2R(E)$, but this value is not constant over the full range of the energy values explored. With our approximation, the $\frac{T_p}{T_e}$ ratio diverges at the transition energy, in fact corresponding to a large value. Therefore, we believe that this term dominates in the q factor around the transition energy. For KC_{24}, the experimental Fermi level shift is 1.05 eV,[43] giving a transition energy of 2.1 eV. Compared to this, our calculations reported in Figure 6 provide a ΔE_F energy value of 0.87 eV, close enough to the experimental value.

As reported in Figure 4, the sign change in q occurs between 1.96 and 1.58 eV. This is quite close to the value determined experimentally for the transition energy and in full

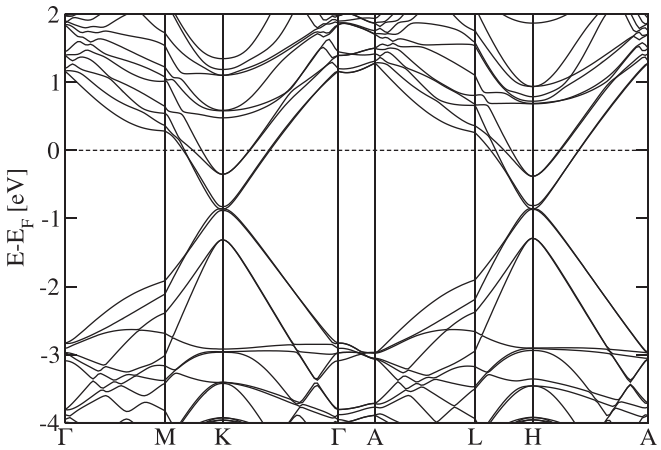

FIG. 6. Calculated electronic band structure of KC_{24}.

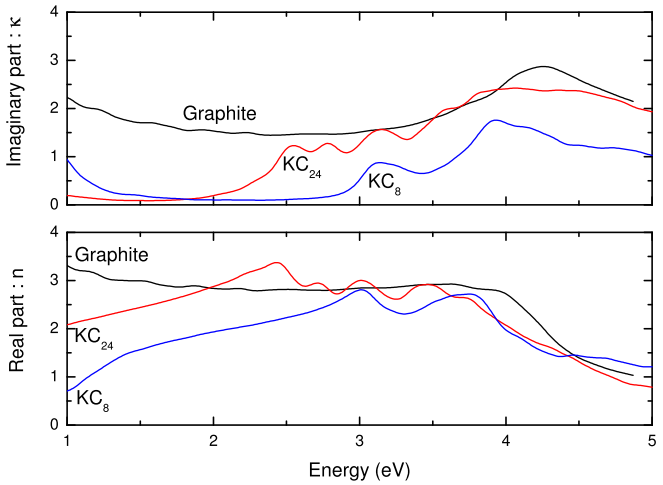

FIG. 7. Optical index (n for the real part and κ for the imaginary part) of graphite, KC_8 and KC_{24}. The absorption coefficient α is related to the imaginary part of the complex index by $\alpha = \frac{4\pi\kappa}{\lambda}$.

agreement with our first principle calculations of the Fermi level shift. It is coming from the charge transfer of the potassium atoms to the graphene layers, 0.75 and 0.78 e^- for KC_8 and KC_{24}, respectively. In order to go further in the interpretation of the electronic band structure, we have also calculated the dielectric constants and then deduced the complex optical index $\tilde{n} = n + i\kappa$. The real and imaginary parts of the optical index are reported in Figure 7. For KC_8, two features at 3.15 eV and 3.95 eV are visible in the imaginary part κ of the optical index and can be related to vertical transitions at Γ points (see Figure 5). For KC_{24}, the behavior is intermediate between graphite and KC_8. For graphite, only one strong absorption maximum is found at 4.25 eV. This 0.3 eV shift has been obtained through Kramers-Kronig analysis of energy-loss spectra.[43] Our finding is fully consistent with these data.

We have also compared these values to the absorbance of graphene solutions, as reported in Figure 8. In the case of KC_8 in NMP, only one strong absorption peak is found (Figure 8, left) consistent with the literature,[1] located at 4.1 eV (300 nm) and corresponding to the second feature in Figure 7. However, it is known that the positions, intensities, and shapes of the absorption bands are usually modified

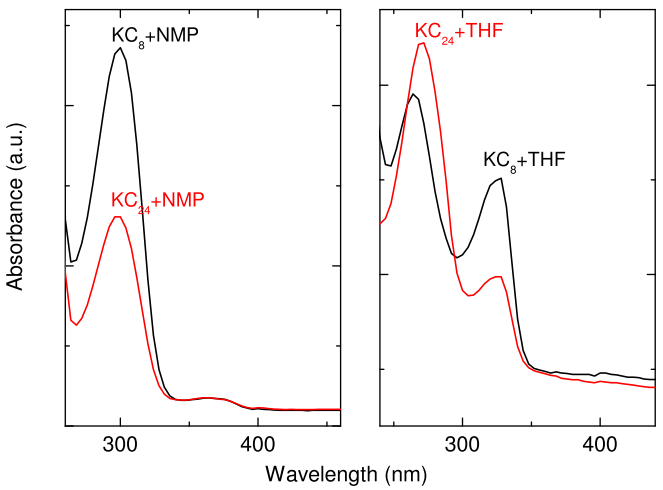

FIG. 8. Absorbance of graphenide solutions in NMP and THF.

when changing the solvent. Correspondingly, in THF, the absorbance (Figure 8, right) presents two clear peaks, a weak one at 3.8 eV (325 nm) and a large one at 4.5 eV (275 nm) with a global shape fitting well with the κ value of KC_8 in Figure 7.

The magnitude of the spectral shifts mainly depends on the strength of the intermolecular hydrogen bonds between the graphenides and the solvent molecules. In many molecules, the $\pi - \pi^*$ bands are shifted bathochromatically (i.e., to lower energy) when the solvent polarity increases. The polarity index of THF and NMP are 4 and 6.7, respectively. Thus, the observed shift of 0.4 eV is consistent with bathochromaticity.[44] For KC_{24}, in the case of NMP, the difference with KC_8 is not straightforward even if the peak intensity ratio (300 nm over the weak peak at 360 nm) could be an indicator.

VI. CONCLUSION

Using multiwavelength Raman scattering, a sign change of the coupling factor involved in the Fano shape was observed for both KC_8 and KC_{24}. This sign change occurs when the excitation energy reaches $2|\Delta E_F| + \hbar\omega_G/2$, thus allowing the shift of the Fermi level to be determined by means of Raman spectroscopy. Then, the two specific features of the absorbance plots of graphenide solutions in two different solvents (NMP and THF) were explained using first principle calculations. The fact that both the position and the intensity of the electronic transitions in graphenide solutions appear to be influenced by the solvent chemical nature might reveal promising characterization issues which should be explored.

ACKNOWLEDGMENTS

Région Midi-Pyrénées and *PRES/Université* de Toulouse are thanked for co-funding the Ph.D. Grant of D. Tristant. The HPCs *CALcul en Midi-Pyrénées* initiative (CALMIP, Grant p0812) is thanked for allocating computational time. Part of the theoretical work was also carried out using GENCI-CINES (Grant 2014-096649), GENCI-CCRT (Grant 2014-096649), and GENCI-IDRIS (Grant 2014-096649) resources. Région Aquitaine is thanked for funding the purchase of laboratory equipment. Dr. Benjamin Levine is acknowledged for careful reading of the manuscript. This work was supported by ANR (ANR-10-BLAN-1003-3 Project "GRAAL"). The work has been performed within the framework of the GDR-I 3217 CNRS "*Graphene & Nanotubes*".

[1]A. Catheline, C. Vallès, C. Drummond, L. Ortolani, V. Morandi, M. Marcaccio, M. Iurlo, F. Paolucci, and A. Pénicaud, "Graphene solutions," Chem. Commun. **47**, 5470 (2011).
[2]T. Enoki, M. Suzuki, and M. Endo, *Graphite Intercalation Compounds and Applications* (Oxford University Press, 2003).
[3]M. S. Dresselhaus and G. Dresselhaus, Adv. Phys. **30**, 139 (1981).
[4]A. Grüneis, C. Attaccalite, A. Rubio, D. V. Vyalikh, S. L. Molodtsov, J. Fink, R. Follath, W. Eberhardt, B. Büchner, and T. Pichler, Phys. Rev. B **80**, 075431 (2009).
[5]A. M. Rao, E. Richter, S. Bandow, B. Chase, P. C. Eklund, K. A. Williams, S. Fang, K. R. Subbaswamy, M. Menon, A. Thess, R. E. Smalley, G. Dresselhaus, and M. S. Dresselhaus, Science **275**, 187 (1997).
[6]R. Krupke, F. Hennrich, H. V. Löhneysen, and M. M. Kappes, Science **301**, 344 (2003).
[7]V. A. Davis, A. N. G. Parra-Vasquez, M. J. Green, P. K. Rai, N. Behabtu, V. Prieto, R. D. Booker, J. Schmidt, E. Kesselman, W. Zhou, H. Fan, W. W. Adams, R. H. Hauge, J. E. Fischer, Y. Cohen, Y. Talmon, R. E. Smalley, and M. Pasquali, Nat. Nanotechnol. **4**, 830 (2009).
[8]P. Puech, T. Hu, A. Sapelkin, I. Gerber, V. Tishkova, E. Pavlenko, B. Levine, E. Flahaut, and W. Bacsa, Phys. Rev. B **85**, 205412 (2012).
[9]A. C. Ferrari, J. C. Meyer, V. Scardaci, C. Casiraghi, M. Lazzeri, F. Mauri, S. Piscanec, D. Jiang, K. S. Novoselov, S. Roth, and A. K. Geim, Phys. Rev. Lett. **97**, 187401 (2006).
[10]A. Eckmann, A. Felten, I. Verzhbitskiy, R. Davey, and C. Casiraghi, Phys. Rev. B **88**, 035426 (2013).
[11]L. G. Canado, A. Jorio, E. H. M. Ferreira, F. Stavale, C. A. Achete, R. B. Capaz, M. V. O. Moutinho, A. Lombardo, T. S. Kulmala, and A. C. Ferrari, Nano Lett. **11**, 3190 (2011).
[12]O. Beyssac, B. Goffé, C. Chopin, and J. N. Rouzaud, J. Metamorph. Geol. **20**, 859 (2002).
[13]N. Rey, P. Toulemonde, D. Machon, L. Duclaux, S. Le Floch, V. Pischedda, J. P. Iti, A.-M. Flank, P. Lagarde, W. A. Crichton, M. Mezouar, Th. Strssle, D. Sheptyakov, G. Montagnac, and A. San-Miguel, Phys. Rev. B **77**, 125433 (2008).
[14]P. C. Eklund, C. H. Olk, F. J. Holler, J. G. Spolar, and E. T. Arakawa, J. Mater. Res. **1**, 361 (1986).
[15]D. E. Nixon and G. S. Parry, J. Phys. D: Appl. Phys. **1**, 291 (1968).
[16]G. Kresse and J. Hafner, Phys. Rev. B **48**, 13115 (1993).
[17]G. Kresse and J. Hafner, Phys. Rev. B **49**, 14251 (1994).
[18]G. Kresse and J. Furthmüller, Comput. Mater. Sci. **6**, 15 (1996).
[19]G. Kresse and J. Furthmüller, Phys. Rev. B **54**, 11169 (1996).
[20]P. E. Blöchl, Phys. Rev. B **50**, 17953 (1994).
[21]G. Kresse and D. Joubert, Phys. Rev. B **59**, 1758 (1999).
[22]G. L. Doll, M. H. Yang, and P. C. Eklund, Phys. Rev. B **35**, 9790 (1987).
[23]M. Dion, H. Rydberg, E. Schröder, D. C. Langreth, and B. I. Lundqvist, Phys. Rev. Lett. **92**, 246401 (2004).
[24]K. Lee, E. D. Murray, L. Kong, B. I. Lundqvist, and D. C. Langreth, Phys. Rev. B **82**, 081101 (2010).
[25]J. Klimes, D. R. Bowler, and A. Michaelides, Phys. Rev. B **83**, 195131 (2011).
[26]R. Bader, *Atoms in Molecules: A Quantum Theory* (Oxford University Press, New York, 1994).
[27]G. Henkelman, A. Arnaldsson, and H. Jonsson, Comput. Mater. Sci. **36**, 354 (2006).
[28]E. Sanville, S. D. Kenny, R. Smith, and G. Henkelman, J. Comput. Chem. **28**, 899 (2007).
[29]W. Tang, E. Sanville, and G. Henkelman, J. Phys.: Condens. Mater **21**, 084204 (2009).
[30]U. Fano, Phys. Rev. **124**, 1866 (1961).
[31]P. C. Eklund and K. R. Subbaswamy, Phys. Rev. B **20**, 5157 (1979).
[32]F. Cerdeira, T. A. Fjeldly, and M. Cardona, Phys. Rev. B **8**, 4734 (1973).
[33]Y. G. Wang, S. P. Lau, B. K. Tay, and X. H. Zhang, J. Appl. Phys. **92**, 7253 (2002).
[34]B. G. Burke, J. Chan, K. A. Williams, Z. Wu, A. A. Puretzky, and D. B. Geohegan, J. Raman Spectrosc. **41**, 1759 (2010).
[35]A. M. Saitta, M. Lazzeri, M. Calandra, and F. Mauri, Phys. Rev. Lett. **100**, 226401 (2008).
[36]J. C. Chacon-Torres, A. Y. Ganin, M. J. Rosseinsky, and T. Pichler, Phys. Rev. B **86**, 075406 (2012).
[37]F. Cerdeira, T. A. Fjeldly, and M. Cardona, Solid State Commun. **13**, 325 (1973).
[38]M. V. Klein, *Light Scattering in Solids I* (Springer, Berlin, Heidelberg, 1983), pp. 147–204.
[39]R. M. Martin and L. M. Falicov, *Light Scattering in Solids I* (Springer, Berlin, Heidelberg, 1983), pp. 79–145.
[40]C. F. Chen, C. H. Park, B. W. Boudouris, J. Horng, B. Geng, C. Girit, A. Zettl, M. F. Crommie, R. A. Segalman, S. G. Louie, and F. Wang, Nature **471**, 617 (2011).
[41]D. M. Basko, New J. Phys. **11**, 095011 (2009).
[42]J. B. Renucci, R. N. Tyte, and M. Cardona, Phys. Rev. B **11**, 3885 (1975).
[43]J. J. Ritsko, Phys. Rev. B **25**, 6452 (1982).
[44]M. Homocianu, A. Airinei, and D. O. Dorohoi, J. Adv. Res. Phys. **2**, 011105 (2011), available at http://stoner.phys.uaic.ro/jarp/index.php/jarp/article/view/56.